J Appl Electrochem (2008) 38:1053–1060
DOI 10.1007/s10800-008-9573-8

ORIGINAL PAPER

Electroless deposited Ni–P alloys: corrosion resistance mechanism

Bernhard Elsener · Maura Crobu · Mariano Andrea Scorciapino · Antonella Rossi

Received: 8 October 2007 / Accepted: 17 April 2008 / Published online: 27 May 2008

Abstract Electroless Ni–P alloys are produced as coatings on a broad variety of substrates. They exhibit a corrosion resistance that is superior to pure nickel but do not form a NiO oxide film (passive film) as pure nickel does. Despite the fact that many mechanisms have been proposed to explain this superior corrosion behaviour, no consensus has yet been reached. In this work electrochemical and XPS surface analytical methods have been combined in order to gain a deeper insight into the mechanisms underlying the corrosion resistance of electroless deposited Ni–P alloys with phosphorus content between 18 and 22 at.%. The anodic polarization curves in acidic and neutral solutions confirm a broad current plateau followed by a region with increasing current density. During potentiostatic polarization in the plateau region the current decays according to a power law with exponent ca. −0.5 indicating diffusion-limited dissolution of nickel. XPS/XAES measurements performed after potentiostatic polarization show that phosphorus is present in three different chemical environments. Based on the Auger parameter concept and on the chemical state plot, the three phosphorus states were assigned to phosphorus in the bulk alloy, phosphates and an intermediate phosphorus compound attributed to elemental phosphorus. Angle-resolved XPS analysis has shown that the elemental phosphorus is enriched at the interface between the alloy and the outermost surface in contact with the corrosive solution. These results suggest the following conclusions: the high corrosion resistance of electroless deposited Ni–P alloys can be explained by a strong enrichment of elemental phosphorus at the interface which limits the dissolution of nickel via a diffusion mechanism. A complementary explanation—not yet advanced—for the high corrosion resistance may lie in the electronic state of nickel in the Ni–P alloys.

Keywords Potentiostatic polarization · Diffusion · Phosphorus enrichment · XPS · Chemical state plot · Auger parameter

B. Elsener · M. Crobu · M. A. Scorciapino · A. Rossi (✉)
Dipartimento di Chimica Inorganica ed Analitica, Università degli Studi di Cagliari, Cittadella Universitaria Monserrato, 09042 Monserrato, CA, Italy
e-mail: rossi@unica.it

B. Elsener · M. Crobu · M. A. Scorciapino · A. Rossi
Unità operativa INSTM, Monserrato, Italy

B. Elsener
Institute for Building Materials, ETH Hönggerberg, ETH Zurich, 8093 Zurich, Switzerland

1 Introduction

The increasing attention toward the outstanding properties of new nano-crystalline materials, has revived interest in Ni–P alloys as far as research and especially challenging technological applications are concerned [1, 2]. These alloys, used in the past chiefly as corrosion protective coatings, constitute the earliest industrial application of X-ray amorphous or nano-crystalline metals, dating back to 1946 [3–5]. Today there is a growing interest in the production of ternary Ni–P alloys [6, 7] and for co-deposition with diamond [8] or PTFE particles [9] in order to produce tailor-made functionalized surfaces.

Ni–P alloys with ca. 20 at.% P (close to the eutectic composition) exhibit distinctly better corrosion resistance than does pure Ni, showing a suppression of anodic dissolution in the potential range where pure nickel dissolves actively in acids [10–22]. This holds for melt spun [10–12], electroless [13–16] or electro-deposited [17–21] Ni–P

alloys. It is also generally accepted that only X-ray amorphous or nano-crystalline alloys—irrespective of mode of production—exhibit this superior corrosion resistance [18–20] whereas (re)crystallization neutralizes this effect [13, 30].

Different models have been proposed for explaining the high corrosion resistance of Ni–P alloys containing more than 18% P:

(1) The formation of a protective nickel phosphate film that acts as diffusion barrier against active dissolution of the alloy [14].
(2) Adsorption of hypophosphite ions, forming a barrier layer that prevents the dissolution of nickel atoms at the alloy surface (called "chemical passivity") [8–11].
(3) The formation of a P-rich film at the alloy/solution interface as a consequence of rapid and selective nickel dissolution [12, 20]. The dissolution process is controlled via diffusion of nickel through this phosphorus-rich zone [10, 12, 19, 20] as also reported for Fe70Cr10P13C7 amorphous alloys [23, 24].

Despite broad agreement on the third point, the exact nature and chemical environment of phosphorus are still under debate. Early work on melt-spun amorphous Ni–P alloys claimed them to be "enriched in elemental phosphorus" [10–12] but assigned phosphorus in the bulk alloy to "elemental phosphorus". This opinion was cited repeatedly until publication of the results of recent work [25, 26]. On the other hand, the authors' work on amorphous Fe70Cr10P13C7 alloys has shown that phosphorus in the bulk of this alloy has a partial negative charge [23, 24] in agreement with the literature data for Ni–P alloys [27, 28] and on a series of binary nickel-phosphides [29]. Thus phosphorus in the bulk of the Ni–P alloy undergoes partial covalent bonding with the metal atoms, influencing both the structural order [29, 30, 31] and the electronic state of nickel in Ni–P compounds and alloys [29, 32, 33].

Information on the phosphorus species present at the surface and on the chemical and surface state thus proves crucial in answering the open question on the high stability of electroless deposited Ni–P alloys. The combined electrochemical and XPS surface analytical study in this work is aimed at identifying the mechanism underlying the high corrosion resistance of electroless deposited Ni–P alloys.

2 Experimental

2.1 Nano-crystalline Ni–P coatings

Ni–P coatings were produced on mild steel substrate in a commercial autocatalytic nickel hypophosphite bath (Ronamax SR) by electroless deposition with a thickness of 10, 15 and 20 μm. The pH of the bath was 4.6–5, temperature was 85–90 °C, the plating time was ca. 2 h. Bath composition and process parameters are reported elsewhere [34, 35]. The surface morphology of the coatings was characterized by light microscopy (MeF3A Reichert Jung), environmental scanning electron microscopy (ESEM, FEI Quanta 600) and atomic force microscopy (AFM—Digital Instruments). The coating composition was determined by ESEM-EDX analysis (Genesis 4000 EDX).

2.2 Electrochemical measurements

All measurements were performed using an EG & G 273 potentiostat–galvanostat controlled by M352 software and Zahner potentiostat–galvanostat (IM6) controlled by an AMOS/ANDI acquisition system. A conventional three-electrode setup was used: The samples (working electrode) were pressed on the side port O-ring seal (diameter 1 cm) in a cylindrical plexiglass cell in order to expose a controlled part of the sample surface to the solution [35]. The counter-electrode was a platinum net separated from the solution by a porous diaphragm. The reference electrode was a saturated calomel electrode (SCE, potential +0.242 V vs. NHE) terminating in a Luggin capillary. All potentials are referred to the SCE electrode.

Potentiodynamic polarization curves (scan rate 0.2 mV s^{-1}) were measured in deaerated near-neutral (pH 6–6.5) 0.1 M NaCl, 0.1 M Na_2SO_4, 0.1 M Na_2SO_4 + 0.1 M NaCl and acidic 0.1 M H_2SO_4 solutions (volume 0.25 dm^3). Specimens were kept at the OCP for 15 min. Potentiostatic polarization was performed using the same setup at potentials −0.1 V SCE and +0.1 V SCE. More details are given in [34, 35].

2.3 Sample preparation for XPS analysis

XPS investigations were performed on samples of about 20 × 20 mm as-received (degreased in ethanol), after mechanical polishing (1200 and 2000-grit paper in water, followed by 9 μm and 1 μm diamond paste in ethanol) and after electrochemical tests. Only the results of samples from potentiostatic polarization are presented in this work. More XPS surface analytical results are presented in a companion paper [36].

Immediately after mechanical polishing and polarization, the samples were transferred to the vacuum chamber avoiding contact with the laboratory atmosphere for longer than 3 min.

2.4 XPS analysis and data processing

XPS analyses were performed with an ESCALAB 200 spectrometer (Vacuum Generator Ltd., U.K.). The X-ray

source was a non-monochromatic Al Kα (1486.6 eV) twin anode run at 20 mA and 15 kV. This source allows measurement of the PKLL line using the Bremsstrahlung. More details on spectra acquisition are given in [31].

The instrument was calibrated using the inert-gas-ion-sputter-cleaned reference materials SCAA90 of Cu, Ag and Au [37]. Sample etching was performed with an Ar^+ ion gun operated at 3 keV and 0.2 mA sample current for 30 s. To compensate for sample charging during the analysis all the binding energies were referred to the carbon 1 s signal at 285.0 eV.

Detailed spectra were processed using the program CASAXPS® software (V3.35, CASA Software Ltd, UK). An iterated Shirley background subtraction was applied before curve-fitting using a linear-least-squares algorithm. A more detailed description of the fitting procedure is provided in [36].

3 Results

3.1 Coating characterization

An optical micrograph of an as-plated sample is given in Fig. 1a, showing the nodular growth of the coating. The AFM map shows the matching interfaces (Fig. 1b) and Fig. 1c shows the frictional image of a 5 × 5 μm area in the flat region. X-ray diffraction showed a broad peak at 44.8°, indicating that the deposits are X-ray amorphous [34, 35]. The broad diffraction pattern was interpreted as the (111) plane of the fcc phase of nickel with crystallite size 1.2 nm [38]. Chemical composition determined by EDX showed a phosphorus content of 18.4–19 at.%, close to the eutectic composition.

3.2 Electrochemical results

The anodic potentiodynamic polarization curves of as-received and mechanically polished Ni–P samples in near-neutral (pH 6–6.5) and acidic solutions (pH 1) are shown in Fig. 2. The reproducibility of replicate experiments in the same system was within ±15%. Two distinct potential ranges can be observed: in the first range from the open circuit potential (OCP) to ca. +0.2 V SCE current density increases very slightly and a current plateau is observed. In the second region at potentials E higher than 0.2 V SCE current density increases rapidly with applied potential. Samples preserve their shiny appearance up to 0.2 V SCE.

Potentiostatic polarization experiments (Fig. 3) in near neutral solutions (pH 6–6.5) at two potentials, −0.1 V and +0.1 V SCE, showed current decays that can be described by a power law with exponent ca. −0.5, indicating a diffusion-limited process. The current density increases

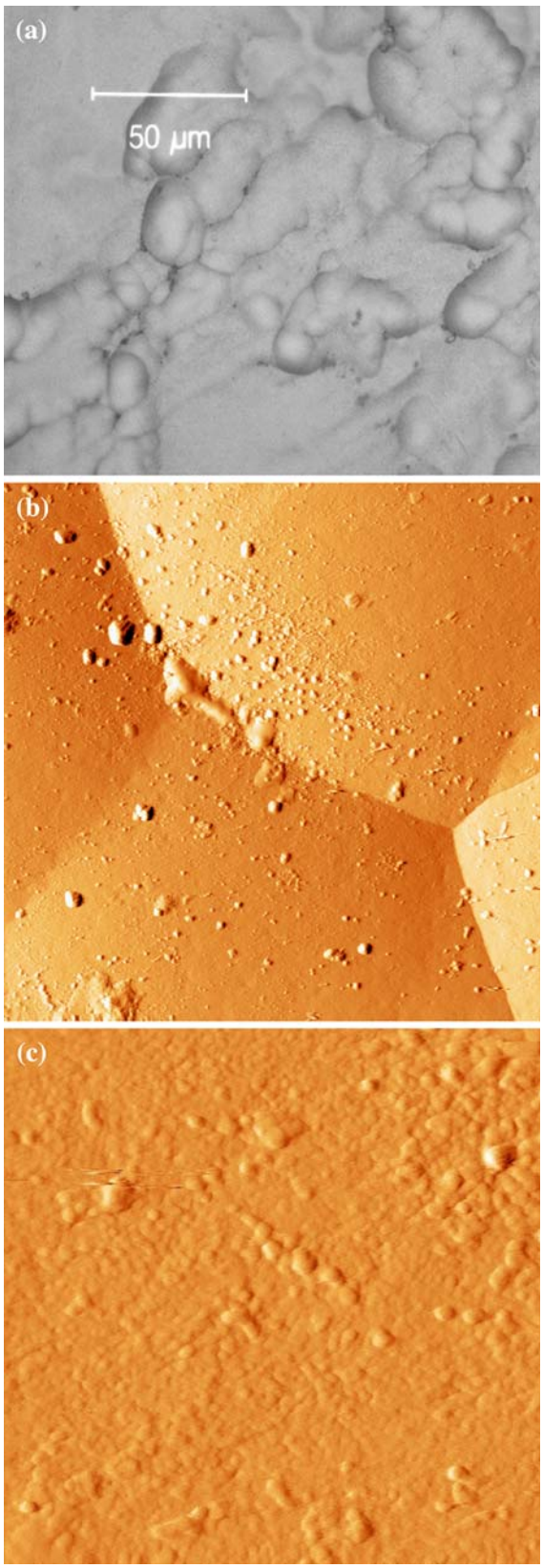

Fig. 1 Surface of as-plated Ni19P alloy (**a**) Micrograph obtained by light microscope, (**b**) AFM map of matching interfaces (10 × 10 μm), (**c**) AFM map of flat region (1 × 1 μm)

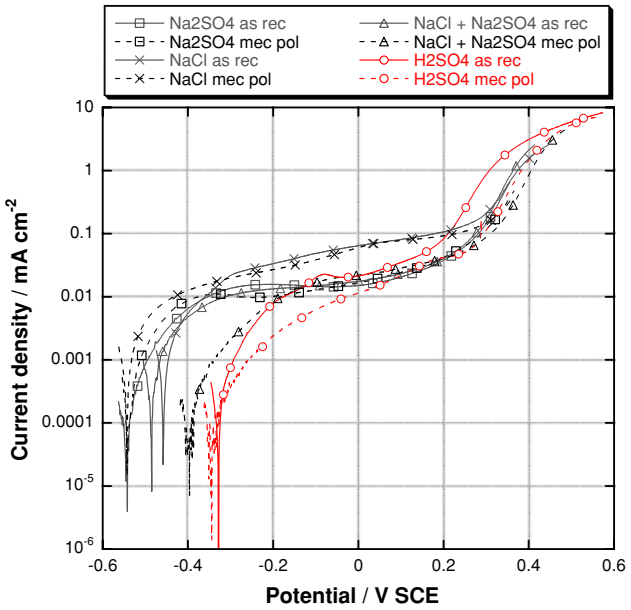

Fig. 2 Anodic polarization curves of as-received and mechanically polished electroless deposited Ni19P alloy in deaerated (N_2 bubbling) near neutral (0.1 M Na_2SO_4, 0.1 M NaCl, 0.1 M Na_2SO_4 + 0.1 M NaCl) and acidic solutions (0.1 M H_2SO4). Scan rate 0.2 mV s^{-1}

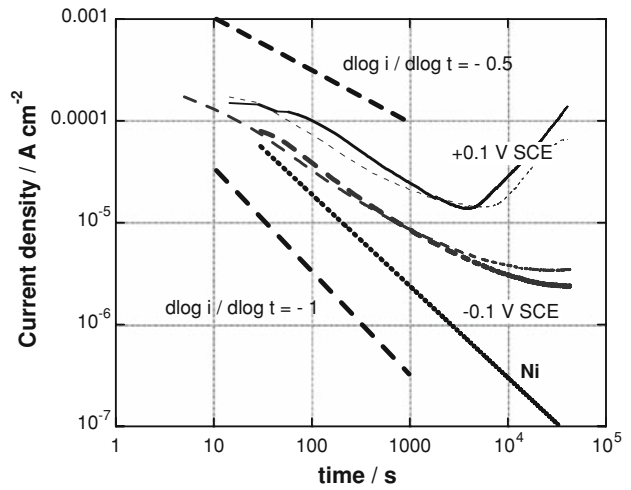

Fig. 3 Potentiostatic polarization curves of electroless deposited Ni19P alloy in deaerated near neutral 0.1 M NaCl solution at potentials of −0.1 V SCE and +0.1 V SCE (in current arrest range, Fig. 2). The curve for pure nickel (−0.1 V SCE, 0.1 M NaCl) is given for comparison

slightly at longer polarization times. This behaviour is associated with the formation of a kind of localized corrosion attack [34, 35], though the origin of this "tunnel structure" [14, 17] is not yet clear.

3.3 XPS/XAES surface analysis

In the survey spectra of sputtered clean Ni–P alloy (not shown) only the signals from photoelectron and X-ray induced Auger peaks of nickel and phosphorus were found. On the as-received samples carbon C1s and oxygen O1s signals were also detected. In the following, the detailed spectra of phosphorus (P2p and PKLL) and nickel Ni2p of a Ni–P sample polarized for 1 h in 0.1 M Na_2SO_4 solution are shown as example. Results of surface analysis of the electroless Ni–P alloy are discussed in detail in a companion paper [36].

3.3.1 Phosphorus

The detailed spectra of phosphorus P2p (Fig. 4a) and corresponding X-ray induced PKLL Auger peak (Fig. 4b) show three different peaks. The most intense P2p signal appears at a binding energy of 129.7 eV and the corresponding PKLL at a kinetic energy of 1858.3 eV. The modified Auger parameter α' calculated as BE(2p) + KE(PKLL) is equal to 1988.1 eV. The phosphorus signal at the binding energy of 133.6 eV and corresponding PKLL signal at 1851.0 eV yields an Auger parameter of 1984.6 eV and can be assigned to phosphates. The third (intermediate) phosphorus signal shows a binding energy of 132.0 eV (Fig. 4a) and a kinetic energy of 1855.4 eV (Fig. 4b). The Auger parameter α' is 1987.3 eV. A correct assignment of the chemical state requires XPS/XAES measurements on standards extensively reported in [36] and the use of the chemical state plot (see Sect. 4).

3.3.2 Nickel

The detailed spectrum of nickel Ni2p3/2 (Fig. 5) is very similar to the typical Ni2p3/2 plus satellite structure as known from pure metallic nickel [33]. The binding energy of the Ni2p3/2 signal is found at 853.0 ± 0.1 eV in good agreement with the literature [11, 33]. The distance of the satellite is found here to be 7.2 eV, thus clearly higher than the 6 eV reported for pure nickel but in keeping with the concept of the influence of phosphorus content on the electronic properties of Ni–P alloys [33]. A very small amount of nickel phosphate (856.4 ± 0.1 eV) is also found. No signals attributable to nickel oxide were detected.

4 Discussion

The mechanism underlying the outstanding corrosion resistance of nano-crystalline Ni–P alloys is still an open question (see Sect. 1). The combination of information from electrochemical results and XPS/XAES surface analytical studies may contribute to identifying that mechanism.

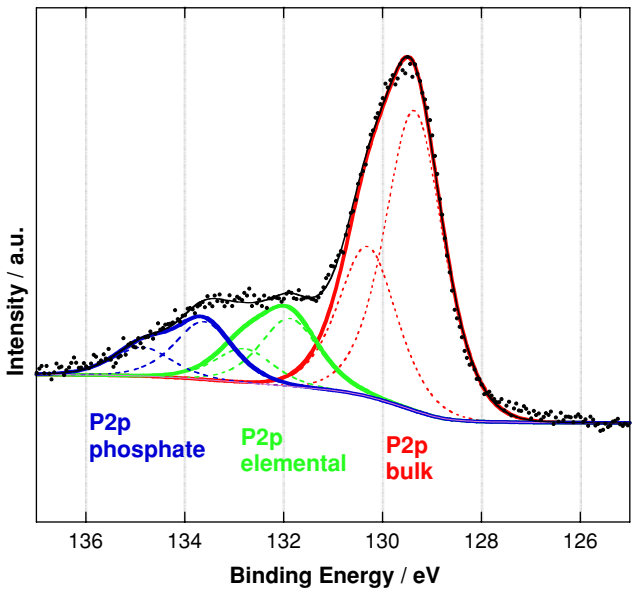

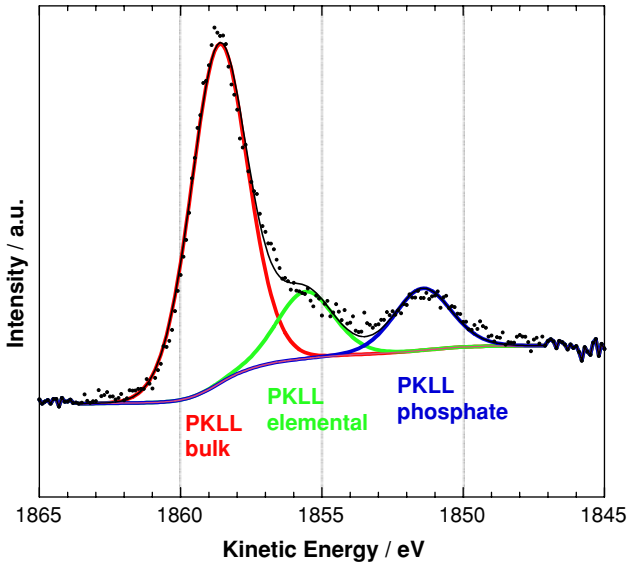

Fig. 4 High resolution XPS P2p and X-ray induced PKLL Auger (XAES) phosphorus spectra of electroless deposited Ni19P alloy after potentiostatic polarization for 1 h at −0.1 V SCE

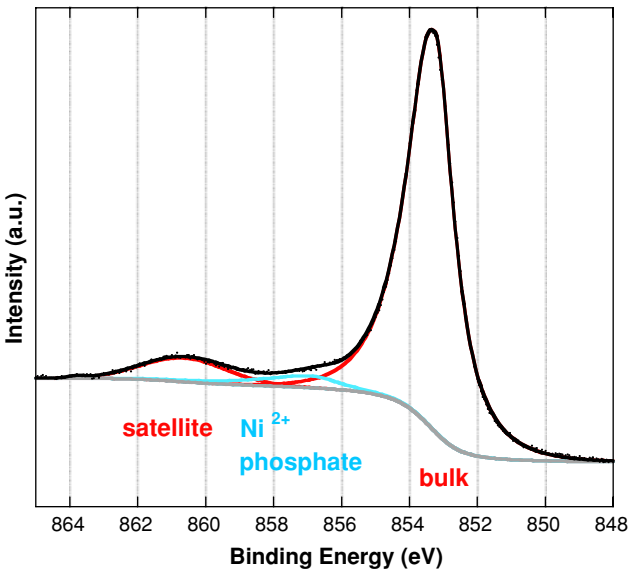

Fig. 5 High resolution XPS Ni2p spectrum of electroless deposited Ni19P alloy after potentiostatic polarization for 1 h at −0.1 V SCE

4.1 Current arrest

The electrochemical results in near neutral and acidic solutions (Fig. 2) confirm the presence of the current plateau or current arrest reported in the literature [10, 12, 19–21]. For the Ni–P alloy studied this occurs in a potential range $-0.2 < E < +0.2$ V SCE where pure nickel exhibits active-to-passive transition [19–21]. As is known, this current plateau and also the current increase at potentials $E > 0.2$ V SCE is practically independent of solution pH [21] and of chloride concentration [19, 20]. This rules out the classical passivation mechanism by oxy-hydroxide formation recognised for pure nickel [39–41] in agreement with XPS surface analytical results, where no nickel oxide was detected on samples potentiostatically polarized in the plateau region (Fig. 5).

4.2 Passivation versus diffusion limitation

Potentiostatic current decay curves of electrodeposited Ni–P alloys in neutral chloride solution [19] and in sulphuric acid [42] exhibit approximately a square root law, the slope of the log i/log t curves being between −0.52 and −0.63 [10, 19, 35, 42]. Ni–P alloys in this work show a similar slope (Fig. 3). The electrochemical results can be interpreted in terms of diffusion of a faster dissolving component of the alloy through the developing surface layer enriched in the less soluble component [11, 12, 19, 20, 35]. Preferential dissolution of Ni from amorphous Ni–P alloys is well documented and the current decay curves may describe the dissolution of nickel limited by diffusion through the P enriched surface layer. However, the chemical state of this phosphorus species is not yet clear.

4.3 XPS/XAES surface analysis: interpretation based on chemical state plot

The results of this study (Fig. 4) reveal three phosphorus peaks associated to three different chemical states. P2p binding energies and PKLL kinetic energies of the three phosphorus species have been reported to be independent of polarization potential [42] and polarization time [35, 36]. The binding energies reported [11, 43] are in good agreement with this work (Table 1). Based on standards of solid phosphorus compounds reported in the literature [23, 44, 45]

Table 1 Measured binding energies of phosphorus P2p compared to reference compounds

Binding energy (eV)	P-species	Alloy	Reference
129.2	P (neutral)	Ni–P 20 RQ	[11, 43]
129.4	P bulk, neg. charged	NiP_3 cryst.	[29]
129.4	P bulk, neg. charged	Fe70Cr10P13C7 RQ	[23]
129.7	P bulk, neg. charged	Ni–P 19 E	This work
132.0	P elemental	Fe70Cr10P13C7 RQ	[23]
132.0	P elemental	Ni–P 21 ED	[42]
132.2	$H_2PO_2^-$	Ni–P 20 RQ	[11, 43]
132.0	P elemental	Ni–P 19 E	This work
133.4	P(V)	Ni–P 21 ED	[42]
133.4	P(V)	Fe70Cr10P13C7 RQ	[23]
133.4	P(V) $Ni_3(PO_4)_2$	Standard	[11, 43]
133.6	P(V) $Ni_3(PO_4)_2$	Standard	[42]
133.5	P(V) $Ni_3(PO_4)_2$	Standard	[44, 45]
133.6	P(V)	Ni–P 19 E	This work

Alloy preparation: rapidly quenched (RQ), electrodeposition (ED), electroless (E)

and analysed in a companion paper [36], the high binding energy peak at 133.6 ± 0.1 eV can be assigned to phosphorus P(V) in phosphates. The most intense peak at 129.7 ± 0.1 eV can be assigned to phosphorus in the bulk alloy, its binding energy being very close to P in binary nickel phosphides [29].

As far as the third (intermediate) species is concerned (binding energy of 132.0 ± 0.1 eV), its chemical state is still under discussion: This species actually exhibits a binding energy higher than elemental P (130.4 eV, [23, 43, 45]) but slightly lower than P^{+1} compounds (NaH_2PO_2 at 132.3 eV) [23, 43, 45]. Considering that phosphorus in phosphates (133.6 eV) has a valence state of P(V) [11, 23, 42–45] and based on the *assumption* that phosphorus in the bulk of the Ni–P alloy has an oxidation state of zero P^0 (called "neutral" [43]) several workers have proposed assigning the intermediate P species to a P(I) or P(III) valence state in an unidentified compound located in the inner part of the passive film of the amorphous alloy [11, 43] or to hypophosphite [11]. Alternatively, this phosphorus species has been assigned to elemental phosphorus P^0 [23, 24].

More precise information on the chemical environment of an element can be obtained employing the (modified) Auger parameter α concept calculated as α = BE (2p) + KE (KLL) [44, 46, 47] and the two dimensional "chemical state plot" based on the Auger kinetic energy and binding energy of the photoelectron line [36, 46, 47]. The three phosphorus species can be found in three distinct regions of the chemical state plot (Fig. 6): the group in the lower left of the plot (P2p3/2 133.6 eV, PKLL 1850.9 eV) corresponds to P(V) in phosphates. This group is close to transition metal phosphates [23, 36, 44, 45]. The points in the upper right region (P2p3/2 129.7 eV, PKLL 1858.3 eV) correspond to P in the bulk alloy as reported for binary nickel phosphides [29], melt spun FeNiPB [44] or FeCr10P13C7 [23]. The intermediate P ($P2p_{3/2}$ 132.0 eV, PKLL 1855.3 eV) occupies the region in the chemical state plot nearest to elemental phosphorus (red or black phosphorus) with Auger parameter 1987.3 eV [29, 44]. These

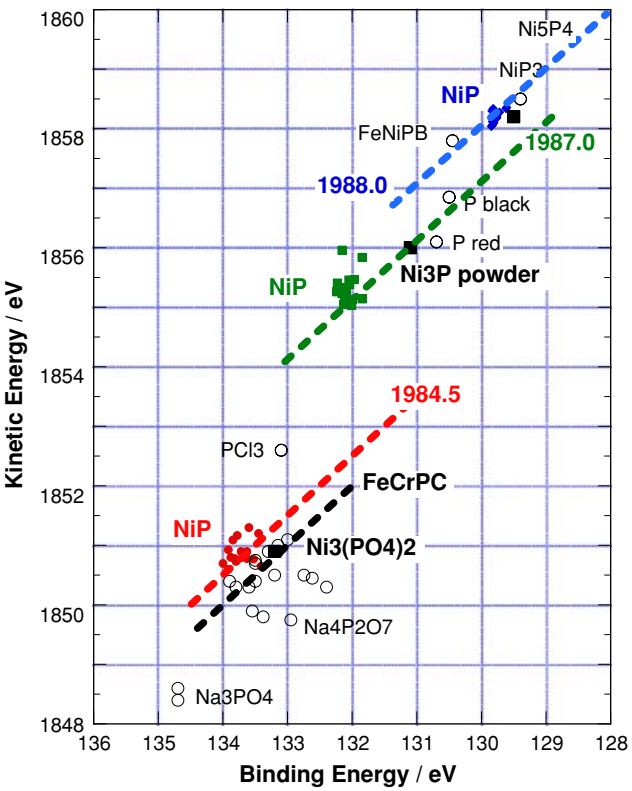

Fig. 6 Chemical state plot of phosphorus showing different P species present on surface of electroless deposited Ni–P alloy. Other P-containing amorphous alloys and reference compounds are given for comparison [29, 36, 44, 45]. Numbers on the diagonal lines represent the Auger parameter α = BE + KE

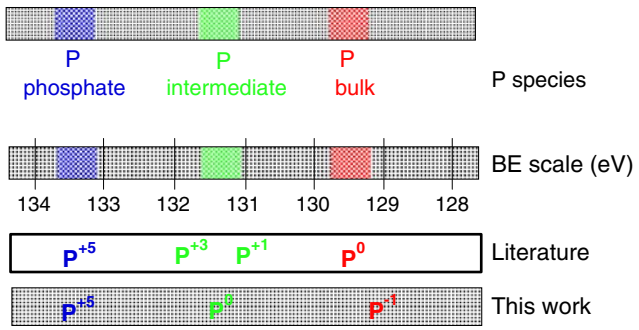

Fig. 7 Schematic drawing of different ways of assigning phosphorus species

results have consequences on the assignments (Fig. 7): (a) as shown for binary nickel phosphides [29], phosphorus in the bulk of the Ni–P alloy is partially negatively charged and cannot be assigned to phosphorus in the valence state P^0; (b) the chemical state of the intermediate phosphorus compound (Fig. 4) is assigned to elemental phosphorus P^0 (in agreement with results from FeCr10P13C7 amorphous alloys [23]), an attribution to P^{+1} (hypophosphite [43]) can be ruled out. The attribution to elemental P is consistent with the finding that its binding energy values remain constant with the applied polarization potential [42].

4.4 Concentration depth profiles—quantitative analysis

Based on the quantitative analysis of the XPS data using the Tougaard algorithm [48], it was possible to determine the in-depth concentration profile of nickel and phosphorus [34, 36]. The theoretical basis and detailed results for this approach are described in a separate paper [36]. The results show (Fig. 8) a pronounced enrichment of phosphorus at the bulk alloy/solution interface, the concentration at the outermost surface increasing with polarization time [34, 36] up to 50% phosphorus. The thickness of the P-enriched layer based on this analysis of XPS data is ca. 1 nm. On top of the alloy a very thin nickel phosphate layer was detected but no nickel oxide [36].

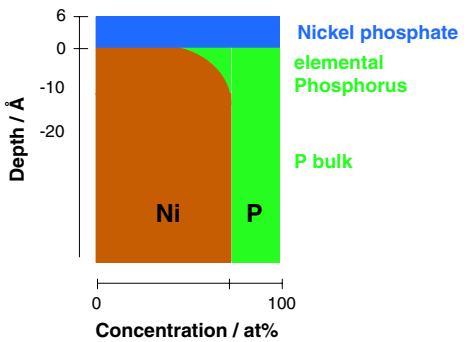

Fig. 8 In-depth profile of phosphorus and nickel at the surface of electroless deposited Ni–P alloy after potentiostatic polarization for 1 h at −0.1 V SCE

4.5 Electronic structure of Ni–P alloys

XPS/XAES measurements have provided evidence of the metallic character of crystalline Ni-phosphides [29]. The high corrosion resistance of Ni–P alloys might be influenced by the electronic structure of these alloys [32] that in turn is affected by phosphorus content [33]. As also shown by the negatively charged (−0.4 eV) phosphorus in the bulk alloy (see above), nickel and phosphorus undergo partial covalent bonding between Ni 3d and P 3p bands [29, 33, 34]. This partial bonding shifts the Ni d band away from the Fermi level to higher binding energies, reducing the Ni density of states (DOS) at E_F (depletion near the Fermi level). Compared to pure nickel, this change in the electronic structure may raise the surface work function, making charge transfer to adsorbed species more difficult, thus enhancing the stability of the Ni–P alloy and its corrosion resistance.

5 Conclusions

From this combined electrochemical and XPS/XAES surface analytical study the following conclusions can be drawn regarding the outstanding corrosion resistance of electroless deposited Ni–P alloys:

- The outstanding corrosion resistance of electroless deposited Ni–19P alloys can be explained by the formation of a phosphorus-enriched layer at the alloy surface. This layer accounts for the diffusion controlled dissolution of the alloy.
- XPS/XAES surface analysis data interpreted on the basis of the Auger parameter concept and the chemical state plot clearly show that phosphorus in this layer has a chemical state close to that of elemental phosphorus.
- Phosphorus in the bulk alloy instead is partially negatively charged and forms chemical bonds with nickel atoms. These chemical bonds might influence the electronic structure and enhance Ni–P alloys resistance to dissolution.
- In agreement with some literature findings no nickel oxide has been detected on the polarized Ni–P alloy, thus an “oxide type” passivity like that observed on pure nickel can be ruled out.

Acknowledgements This work was funded by the University of Cagliari. We gratefully acknowledge the award of a Ph.D. fellowship to M.A. Scorciapino by the Italian Ministry for Education, University and Research (MIUR). The authors wish to thank Galvanic AG,

Wädenswil (Switzerland) who supplied the electroless deposited NiP alloys and Gaby Peschke of ETH Zurich, Institute of Building Materials, for performing the ESEM/EDX measurements. Thanks are also due to Dr. Tanja Drobek (LSST—ETH Zürich) who performed the AFM measurements.

References

1. Haidu J (1997) Trans Inst Met Finish 75:B7
2. Grimsley S (2002) Trans Inst Met Finish 80:B4
3. Brenner A, Riddel GE (1946) In: Proceedings of the AES 33rd Annual Conference, p 23
4. Brenner A, Couch EG, Williams EK (1950) J Res NBS 44:109
5. De Minjer CH, Brenner A (1957) Plating 44:1297
6. Balaruja JN, Sankara N, Seshardri SK (2003) J Appl Electrochem 33:807
7. Balaruja JN, Ezhil Selvi V, William Grips VK, Rajam KS (2006) Electrochimica Acta 52:1064
8. Xiang Y, Zhang J, Jin C (2001) Plat Surf Finish 88:64
9. Duncan RN (1989) Met Finish 87:33
10. Diegle RB, Sorensen NR, Nelson GC (1986) J Electrochem Soc 133:1769
11. Diegle RB, Sorensen NR, Clayton CR, Helfand MA, Yu YC (1988) J Electrochem Soc 135:1085
12. Habazaki H, Ding SQ, Kawashima A, Asami K, Hashimoto K, Inoue A, Matsumoto T (1989) Corros Sci 29:1319
13. Parente MMV, Mattos OR, Diaz SL, Lima NP, Fabri Miranda FJ (2001) J Appl Electrochem 31:677
14. Salvago G, Fumagalli G, Brunella F (1989) Surf Coat Technol 37:449
15. Totlani MK, Athavale SN (2000) Corros Rev 18:155
16. Hari Krishnan K, John S, Srinivasan KN, Praveen J, Genasan M, Kavimani PM (2006) Metall Mater Trans A 37:1917
17. Salvago G, Fumagalli G (1987) Met Finish 85:31
18. Ratzker M, Lashmore DS, Pratt KW (1986) Plat Surf Finish 76:74
19. Krolikowski A (1994) Passive characteristics of amorphous Ni–P alloys. In: Marcus P, Baroux B, Keddam M (eds) Modifications of passive films. The Institute of Materials, London, pp 119–122
20. Krolikowski A (1995) Mater Sci Forum 185–188:799
21. Krolikowski A, Karbownicka B, Jaklewics O (2006) Electrochim Acta 51:6120
22. Burstein GT (1981) Corros NACE 37:549
23. Rossi A, Elsener B (1994) Characterization of surface films on FeCrPC alloys by XPS and X-ray excited Auger peaks. In: Marcus P, Baroux B, Keddam M (eds) Surface modifications of passive films. EFC Publication No. 12, The Institute of Materials, London, pp 6–11
24. Elsener B, Rossi A (1997) Metall Foundry Eng 23:157
25. Splinter SJ, Rofagha R, McIntyre NS, Erb U (1996) Surf Interface Anal 24:181
26. Peeters P, Hoorn G, Daenen T, Kurowski A, Staikov G (2001) Electrochimica Acta 47:161
27. Asami K, Rimura HM, Hashimoto K, Masumoto T, Yokoyama A, Komiyama H, Inoue H (1984) J Non-Cryst Solids 64:149
28. Chen N, Feng P, Sun J (1985) The electronic structure of Ni–P and Pd–Ni–P glasses. In: Steeb S, Warlimont H (eds) Rapidly quenched metals. Elsevier Science Publisher B.V., pp 999–1002
29. Franke R (1997) Spectrochimica Acta A 53:933
30. Hausleitner Ch, Hafner J (1993) Phys Rev B 47:5689
31. Elsener B, Atzei D, Krolikowski A, Rossi Albertini V, Sadun C, Caminiti R, Rossi A (2004) Chem Mater 16:4216
32. Kojno J, Szasz A, Krasser W, Mark G, Stepanjuk VS, Katsnelson AA (1992) J Phys Condens Matter 4:2487
33. Elsener B, Atzei D, Krolikowski A, Rossi A (2008) Effect of phosphorus concentration on the electronic structure of Ni–P nano-crystalline electrodeposited alloys: an XPS and XAES investigation. Surf Interface Anal. doi:10.1002/sia.2802 (Published online 20 February 2008)
34. Crobu M (2007) Tesi di Laurea (Master Thesis). University of Cagliari
35. Crobu M, Scorciapino A, Elsener B, Rossi A (2008) Electrochimica Acta 53:3364
36. Scorciapino A, Crobu M, Elsener B, Rossi A XPS/XAES analysis of nano-crystalline Ni–P alloys (in preparation)
37. Surface Chemical Analysis–X-ray Photoelectron Spectrometers–Calibration of Energy Scales (2001) ISO 15472:2001. International Organization for Standardization, Geneva, Switzerland
38. Révész A, Lendvai J, Loranth J, Padar J, Bakonyi IJ (2001) J Electrochem Soc 148:C715
39. MacDougall B, Mitchell DF, Graham MJ (1982) Corrosion 38:85
40. Sikara E, MacDonald DD (2002) Electrochimica Acta 48:69
41. Hoppe HW, Strehblow HH (1990) Surf Interface Anal 16:271
42. Rossi A, Atzei D, Elsener B, Krolikowski A (2001) Electrochemical and XPS surface analytical characterization of amorphous electrodeposited NiP alloys. Proceedings of the EUROCORR 2001. Associazione Italiana Metallurgia (AIM), Milan (on CD)
43. Diegle RB, Clayton CR, Lu Y, Sorensen NR (1987) J Electrochem Soc 134:138; Diegle RB, Clayton CR, Lu Y, Sorensen NR (1986) Evidence of chemical passivity in amorphous Ni–20P alloy. In: Mc Cafferty E, Brodd RI (eds) Surface, inhibiton and passivation. The Electrochemical Society, Pennington, pp 289–303
44. Franke R, Chassé Th, Streubel P, Meisel A (1991) J Electron Spectrosc Relat Phenom 56:381
45. Chassé T, Franke R, Urban C, Franzheld R, Streubel P, Meisel A (1993) J Electron Spectrosc Relat Phenom 62:237
46. Wagner CD, Joshi A (1991) J Electron Spectrosc Relat Phenom 47:283 and references quoted therein
47. Moretti G (1998) J Electron Spectrosc Relat Phenom 95:95
48. Tougaard S (1997) Surf Interface Anal 25:137